ACS APPLIED MATERIALS & INTERFACES

www.acsami.org

Research Article

Optimization of Polyelectrolyte Coacervate Membranes via Aqueous Phase Separation

Shao-Hsiang Joe Hung, Meng-Chen Chiang, and Jessica D. Schiffman*

Cite This: https://doi.org/10.1021/acsami.4c18989

Read Online

ACCESS | Metrics & More | Article Recommendations | Supporting Information

ABSTRACT: Polymeric membranes fabricated via the nonsolvent-induced phase separation process rely heavily on toxic aprotic organic solvents, like *N*-methyl-pyrrolidine (NMP) and dimethylformamide. We suggest that the "saloplastic" nature of polyelectrolyte complexes (PECs) makes them an excellent candidate for fabricating next-generation water purification membranes that use a more sustainable aqueous phase separation process. In this study, we investigate how the properties of PECs and their interactions with salt can form pore-containing membranes from the strong polyelectrolytes poly(sodium 4-styrenesulfonate) (PSS) and poly(diallyldimethylammonium chloride) (PDADMAC) in the presence of potassium bromide (KBr). How the single-phase polymer-rich (coacervate) dope solution and coagulation bath impacted the formation, morphology, and pure water permeance (PWP) of the membranes was systematically evaluated by using scanning electron microscopy and dead-end filtration tests. The impact of a salt annealing post-treatment process was also tested; these treated PEC membranes exhibited a PWP of 6.2 L m^{-2} h^{-1} bar^{-1} and a dye removal of 91.7% and 80.5% for methyl orange and methylene blue, respectively, which are on par with commercial poly(ether sulfone) nanofiltration membranes. For the first time, we have demonstrated the ability of the PEC membranes to repel *Escherichia coli* bacteria under static conditions. Our fundamental study of polyelectrolyte membrane pore-forming mechanisms and separation performance could help drive the future development of sustainable materials for membrane-based separations.

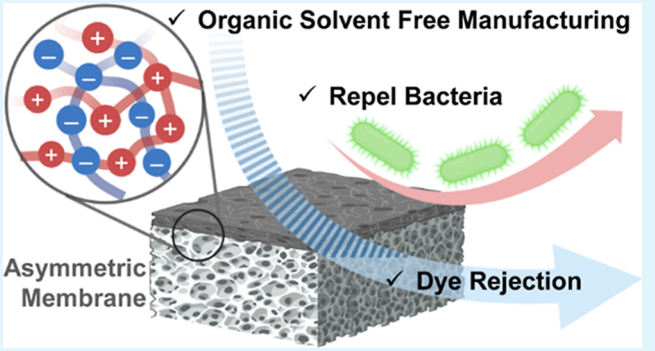

KEYWORDS: *antifouling, charged polymers, dye rejection, phase inversion, sustainability, salt annealing*

INTRODUCTION

According to the World Health Organization, in 2021, over 2 billion people were living in water-stressed countries.[1] Access to clean water will remain a major challenge for the foreseeable future due to climate change and population growth, which will further exacerbate this problem. Currently, membrane-based reverse osmosis (RO) processes are the most reliable method of producing clean water through desalination.[2] Since its invention in the 1960s, nonsolvent-induced phase separation (NIPS) has been an industrial workhorse for fabricating asymmetric polymeric membranes for filtration applications, ranging from RO to dialysis.[3,4]

During the NIPS process, the membrane-forming polymer is dissolved in an organic solvent that is miscible with water, which is used as the nonsolvent. The polymer solution is then cast, immersed, and precipitated in a nonsolvent water bath, where the solvent and nonsolvent exchange is initiated. Based on the tunable interaction between the three-phase system—polymer, solvent, and nonsolvent—past research has manipulated the membrane structure and its corresponding separation performance.[5−7] A significant drawback of the NIPS process is that the commonly used solvents, such as *N*-methyl-2-pyrrolidone (NMP), are reprotoxic and require an expensive recycling process. The membrane industry produces ∼50 billion liters of NMP and *N*,*N*-dimethylformamide (DMF) contaminated wastewater per year[8] and, thus, is under increasing scrutiny by the European Chemical Agency and the United States Environmental Protection Agency.[9,10] Therefore, alternative membrane chemistries that do not rely on toxic solvents are needed.

Polyelectrolyte-rich liquids that form due to the electrostatic complexation of oppositely charged polymers in water are called complex coacervates.[11] The self-assembly of these dense liquids is due to electrostatics, entropy, and parameters, i.e., ionic strength, pH value, polymer chemistry, polymer chain length, and relative concentration of the charged polymers, which can be used to control their interactions.[12,13] While

Received: November 1, 2024
Revised: December 10, 2024
Accepted: December 10, 2024

liquid coacervates have seen many applications, including personal care and food products,[14] more recently, research into the processing of solid polyelectrolyte complex (PEC) materials has grown in popularity. Due to the "saloplasticity" of PEC materials, meaning that they can be plasticized and processed using salt and water,[15−17] several manufacturing techniques, such as hot-pressing, bar coating, layer-by-layer deposition, spin coating, electrospinning, and 3D printing,[18,19] have been used to process PECs into multilayer films,[20,21] cargo-containing nanofibers,[22] anion-exchange membranes,[23] zinc-air batteries,[24] cell scaffolds,[25] and food packaging.[26] Additionally, PEC asymmetric water filtration membranes have been realized and offer a more sustainable manufacturing approach.[27,28]

The process, termed aqueous phase separation (APS), indicates that water can serve as both the solvent and nonsolvent when PECs are used to prepare asymmetric porous membranes.[29,30] For example, De Vos' group triggered phase transition from a liquid state to a solid membrane by changing the pH value or the salt concentration in the coagulation bath. Shifting the pH value in the presence of at least one weak polyelectrolyte has been demonstrated to initiate the complexation utilized to fabricate flat sheet membranes,[31,32] hollow fiber membranes,[30,33] natural polyelectrolyte membranes,[34] and responsive copolymer membranes.[35] However, the huge pH shift (i.e., from pH 12 to 4) requires special equipment and, thus, is less amenable to scale-up. On the other hand, by capitalizing on their saloplasticity, the salinity-induced method showed great similarity with the traditional NIPS process, except an aqueous salt solution in the salinity-induced APS process replaces the aprotic organic solvent. Dope solutions that contain strong polycations, strong polyanions, and a high salt concentration can be precipitated in a lower salinity coagulation bath where the polyelectrolyte complexation is triggered by salt ion removal. Recent work utilizing this method has demonstrated how key parameters, such as polyanion/polycation monomer ratio,[36−38] coagulation bath composition,[29,39] polymer concentration, and molecular weight,[29,40] influence membrane structures and their separation performance. Microfiltration to nanofiltration membranes have been successfully fabricated, and their corresponding separation using humic acid and salt retention have been demonstrated. However, there was limited control over the membranes' morphology, and they demonstrated low pure water permeance (PWP) (<2 L m^{-2} h^{-1} bar^{-1}) and defects. Several methods to improve membrane performance, for example, incorporating pore formers,[40] tuning hydrophobicity,[40] and cross-linking,[36] have been reported, but surface defects have remained. Notably, to date, only one study has utilized the polymer-rich coacervate phase as the dope solution.[40] However, many questions remain, including how the composition of the membrane casting dope and postprocessing of the formed membrane influences its pore-forming pathway and subsequent performance.

In this study, we present the fabrication of PEC membranes from salinity-induced phase separation using a single-phase polymer-rich coacervate as the casting dope solution. For the first time, the canonical, strong polyelectrolyte system of poly(sodium 4-styrenesulfonate) (PSS) and poly(diallyl dimethylammonium chloride) (PDADMAC), with the presence of potassium bromide (KBr) was used to form the homogeneous coacervate solution that was cast into a flat sheet membrane. We explored the role of the coacervate composition and coagulation bath salinity on the final membrane structure. While salt annealing has previously been demonstrated to reduce surface roughness and enhance the stability and salt rejection of polyelectrolyte multilayers (PEMs),[41−43] postprocessing via salt annealing has not yet been explored for improving the performance of membranes cast using APS. Here, we postprocessed the PEC membranes using salt annealing to address persistent defects in PEC membranes. The PWP and removal of charged dyes and neutral poly(ethylene glycol) solutes by the as-prepared and salt-annealed PEC membranes were evaluated. Additionally, the static antifouling properties of the PEC membranes were evaluated using *Escherichia coli* K12.

EXPERIMENTAL SECTION

Materials and Chemicals. All chemicals were used as received. Poly(sodium 4-styrenesulfonate) (PSS, 30 wt %, average M_w ~ 200,000 Da) and poly(diallyldimethylammonium chloride) (PDADMAC, 20 wt %, M_w 200,000−350,000 Da) were purchased from Sigma-Aldrich and used as the polyanion and polycation, respectively. Methylene blue (MB) with a chloride counterion (MB, Biological Stain Commission), glycerol (>99.5%), M9 minimal salts (M9 media), tryptone, and yeast extract were also purchased from Sigma-Aldrich. Potassium bromide (KBr, ACS grade) and methyl orange (MO) with a sodium counterion (MO, ACS grade) were purchased from Thermo Scientific. Poly(ethylene glycol) (PEG) of different molecular weights (600, 1000, 2000 Da) were purchased from Polymer Source, Inc. (QC, Canada). Plastic pH indicator strips, sodium chloride (NaCl, Granular/USP/FCC), and poly(ether sulfone) (PES) 1000 molecular weight cutoff (MWCO) membranes (Sartorius) that were used as controls, were purchased from Fisher Scientific. Spectinomycin dihydrochloride pentahydrate (USP grade) was purchased from Gold Biotechnology (Olivette, MO). Deionized (DI) water was obtained from a Barnstead Nanopure Infinity water purification system (Thermo Fisher Scientific, Waltham, MA). Membranes were hand-cast onto Hollytex grade 3324 nonwoven filter paper purchased from Kavon Filter Products Co (Wall Township, NJ). *E. coli* K12 MG1655 (*E. coli*) was purchased from DSMZ (Leibniz-Institut, Germany).

Coacervate Preparation. Individual PSS and PDADMAC stock solutions were prepared gravimetrically at a concentration of 1 M with respect to the monomer units. KBr stock solution was prepared at a concentration of 4 M. A complex coacervate was prepared by mixing a KBr stock solution with water in a beaker, followed by sequential addition of PSS and PDADMAC stock solutions. The PSS and PDADMAC monomer ratio was 1:1 at a total PEC concentration of 0.4 M for all of the samples. The KBr concentrations in the mixture were prepared at three different concentrations: 1.4, 1.5, and 1.6 M. The mixture was stirred for 24 h to form a homogeneous solution before being poured into a 500 mL separatory funnel. After 14 days, the coacervate phase was completely phase separated from the supernatant phase and stored in 50 mL centrifugal tubes at room temperature until use. The coacervate was very stable and was used over 6 months after collection without a detrimental impact on the membrane formation process.

Membrane Fabrication. The membranes were cast using a method that was previously used to make polysulfone membranes that act as a support for thin-film composite membranes.[44] The viscous coacervate phase, where KBr was prepared at different concentrations, was hand-cast onto a 10.2 cm × 15.3 cm Hollytex nonwoven filter paper, which was secured using tape (Scotch Magic tape, 3 M) to a glass plate (17.8 cm × 25.4 cm). A casting knife (5.08 × 5.08 cm, Gardco Inc., Pompano Beach, FL) with a gate height of 10 mil (0.254 mm) was used to spread the coacervate into a thin layer on the glass plate. After casting, the whole assembly was immediately immersed in a DI water coagulation bath that contained either 0, 0.2, or 0.4 M $KBr_{(aq)}$ for 1 h at room temperature. The as-prepared membranes were rinsed 3 times with DI water before being stored in a DI water

https://doi.org/10.1021/acsami.4c18989
ACS Appl. Mater. Interfaces XXXX, XXX, XXX−XXX

bath overnight at room temperature to encourage the residual salt to diffuse out from the membranes before use. The nomenclature of the membranes presented in this work is summarized in Table 1.

Table 1. Precursor Compositions for Membranes Prepared in This Work by APS, Including the KBr Concentration (C_{KBr}) in the Coacervate Dope Solution and Coagulation Bath

coacervate dope solution C_{KBr} (M)	coagulation bath C_{KBr}		
	0 $M_{(aq)}$	0.2 $M_{(aq)}$	0.4 $M_{(aq)}$
1.4[b]	[a]	[a]	1.4/0.4
1.5	1.5/0	1.5/0.2	1.5/0.4
1.6[b]	[a]	[a]	1.6/0.4

[a]Membranes fabricated from these conditions had minimal permeance or were not mechanically stable enough to evaluate and therefore, were not a focus of this article. [b]KBr concentrations less than 1.4 M were too viscous to be cast. KBr concentrations greater than 1.6 M were not viscous enough (too runny) to enable stable casting.

Salt annealing of the as-prepared membranes was also explored. Here, the as-prepared membranes were immersed in a 1.6 M NaCl solution for 16 h, followed by DI water rinsing 3 times before storage in a DI water bath at room temperature. Three coupons (2.54 cm diameter circle) were punched from each hand-cast membrane sheet using a Spearhead 130 Power Punch MAXiset (Fluid Sealing Services, Wausau, WI). All membranes were used within 14 days of fabrication to prevent potential contamination.

Membrane Characterization. When wet, the membrane's thickness (Z) was measured at five locations on every membrane coupon before and after filtration using a Mitutoyo 293−330 digital micrometer (Toronto, Ontario, Canada). The fabricated membranes' surface morphology and cross-sectional structure were examined by a scanning electron microscope (FEI Magellan 400 XHR-SEM, ThermoFisher Scientific, Hillsboro, OR). Membranes for scanning electron microscopy (SEM) analysis were cast directly onto plastic sheets. Free-standing membranes were peeled off of the plastic sheet before being immersed in 20% w/v glycerol solution overnight to prevent their pores from collapsing. Next, the membranes were immersed in liquid nitrogen, fractured, and placed on flat 90° stubs to obtain both top-down and cross-sectional SEM images. Samples were sputter-coated (Cressington 108 Sputter Coater, Watford, UK) with 6 nm of gold before imaging. The bulk thickness and skin layer thickness of the dry as-prepared membranes were analyzed using ImageJ software[45] for at least 10 locations from three separate cross-sectional SEM images.

The surface zeta potential of the membrane was measured using a Zetasizer Nano ZSP with a surface zeta potential cell (Malvern Panalytical, MA). Membrane samples were glued onto the surface zeta potential cell with epoxy (Loctite Epoxy Instant Mix) and immersed in a tracer solution. The tracer solution for anionic samples was purchased from Malvern Panalytical (ZTS1240, pH = 7), whereas diluted Downy fabric softener solution (0.8 μL/mL H_2O, pH = 5) was used for the cationic sample, as suggested by Ana Morfesis at Malvern Panalytical. The mobility of the tracer particles measured is the balance between electro-osmosis and electrophoresis motion. Measurements were acquired at 125, 250, 375, 500, and 1000 μm distances from the sample surface. The final measurement at 1000 μm was an electrophoresis-only measurement to determine the zeta potential of the tracer particles. By plotting the reported zeta potential as a function of displacement from the surface, the membrane surface zeta potential can be extrapolated and calculated using eq 1

$$\text{surface zeta potential(mv)} = -\text{intercept} + \text{tracer zeta potential} \quad (1)$$

Membrane surface topography images were acquired using a Cypher ES atomic force microscope (Asylum Research/Oxford Instruments, Santa Barbara, CA). Samples were scanned in water using alternating current mode and the OPUS AC-240 (k = 2 N/m) probe (NanoAndMore, Watsonville, CA). Before scanning, the probe was thermally calibrated in air to determine its spring constant (k = 2 N/m) and its resonance frequency (~65 kHz) using the blue drive. Subsequently, the probe was moved to the hydrated surface and confirmed to be fully submerged in water before thermal calibration was applied again to obtain the lever sensitivity underwater with the constant spring constant (k = 2 N/m). After acquiring lever sensitivity, the probe was tuned with a drive amplitude (9 mW) to receive frequency underwater (~25 kHz). When the scans were completed, the topographical images of hydrated membranes were analyzed with IgorPro (WaveMetrics, Inc., Lake Oswego, OR) to quantify the surface roughness including root-mean-square roughness (R_q), average roughness (R_{avg}), skewness (R_{skw}), kurtosis (R_{kurt}), minimum roughness (R_{min}), and maximum roughness (R_{max}).[46] Measurements were collected on 3 samples each for the as-prepared, salt-annealed, and Sartorius control membranes.

PWP and PEG Rejection. Membrane filtration was conducted using a 10 mL dead-end stirred cell (Sterlitech, Auburn, WA). The effective membrane area reported by the manufacturer was 3.5 cm^2. The stirred cell was pressurized by using a nitrogen tank, where the transmembrane pressure (TMP) was measured by using a digital pressure gauge purchased from Cole-Palmer. All membranes were compacted for 1 h at 3 bar of TMP to achieve steady water flux before further testing. For PWP measurements, the permeate weight (M) was recorded at 15 min intervals for 1 h using a digital weighing scale (U.S. Solid, Cleveland, OH). The PWP reported was an average over the 1 h test and determined using eq 2

$$\begin{aligned}\text{PWP}(\text{Lm}^{-2}\text{h}^{-1}\text{bar}^{-1}) &= \frac{J(\text{Lm}^{-2}\text{h}^{-1})}{\text{TMP(bar)}} \\ &= \frac{M(\text{kg})}{\rho(\text{kg L}^{-1})A(\text{m}^2)\Delta t(\text{h})}/\text{TMP(bar)}\end{aligned} \quad (2)$$

where J is the pure water flux, ρ is the density of water, A is the effective membrane area, and Δt is the measurement time. For each casting condition, at least six membrane samples were tested.

PEG rejection measurements were performed separately with three molecular weights (600, 1000, and 2000 Da) using a PEG feed concentration of 1 g/L for each molecular weight. Membranes were first compacted before being tested at 3 bar of TMP until 4 mL of permeate was collected. Feed and permeate solutions were dried and redissolved in an eluent consisting of 80/20 0.1 M sodium nitrate/acetonitrile solution for analysis using gel permeation chromatography with a size exclusion column (Agilent 1200/1260 Infinity GPC/SEC series). The solution flow rate was 1 mL/min and went through three Waters Ultrahydrogel Linear Columns (WAT011545, 10 μm, 7.8 × 300 mm^2) in series. In order to calculate the PEG concentration, calibration curves for each molecular weight of PEG were prepared. PEG rejection was calculated using eq 3

$$\text{PEG rejection}(\%) = \left(1 - \frac{C_p}{C_f}\right) \times 100 \quad (3)$$

where C_p and C_f are the permeate and feed PEG concentrations, respectively. For each casting condition, at least three membrane coupons were tested.

Dye Adsorption Test. Single-component adsorption tests were performed by immersing a membrane coupon (1.57 cm diameter circle) into 5 mL of 12.5 ppm of MO or MB solution. All MO and MB solutions had a pH value of 5, measured using plastic pH indicator strips. The membrane mass was recorded before it was secured using tape to the base of a well within a 12-well plate, where the absorbance of the dye solution in each well was measured using a BioTek Synergy HTX Multimode Reader. The adsorption was studied for 24 h; the first hour was measured in 15 min intervals, followed by

https://doi.org/10.1021/acsami.4c18989
ACS Appl. Mater. Interfaces XXXX, XXX, XXX−XXX

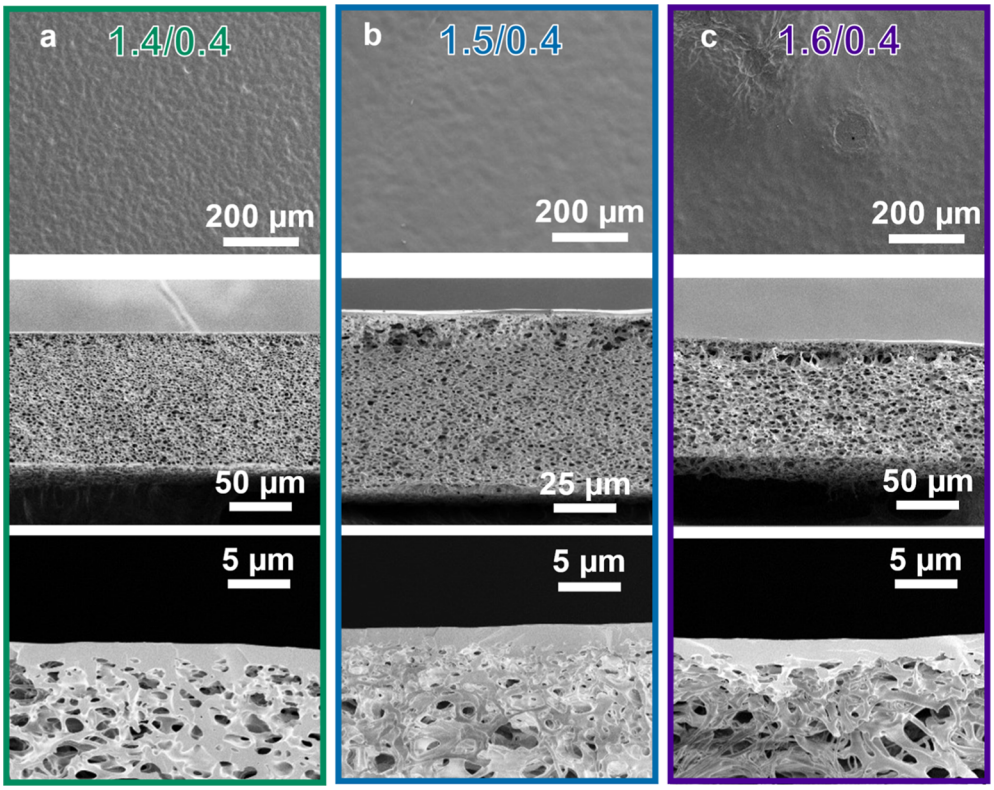

Figure 1. (top row) Top-down, (middle row) cross-sectional, and (bottom row) enlarged cross-sectional SEM micrographs of the PSS/PDADMAC membranes prepared from varied coacervate KBr concentrations: (a) 1.4, (b) 1.5, and (c) 1.6 M in a 0.4 M $KBr_{(aq)}$ coagulation bath. Dry membrane and skin layer thickness are summarized in Table S2. Additional close-up cross-sectional micrographs are provided in Figure S1.

60 min intervals. The dye adsorption percent was calculated using eq 4

$$\text{adsorption}(\%) = \left(1 - \frac{A_a}{A_b}\right) \times 100 \quad (4)$$

where A_b and A_a are the dye solution absorbance before and after adsorption, respectively.

Steady-State Dye Rejection Performance. To characterize the selectivity of our membranes, we filtered a 100 mg/L aqueous solution containing equal concentrations of MO and MB dyes through our membranes using the dead-end stirred cell at 3 bar for 2 h. The feed solution was stirred at 600 ppm to minimize concentration polarization. To obtain steady-state separation performance, all membranes were saturated in the feed solution for 24 h before testing to eliminate the contribution of adsorption from dye removal. The first hour of the filtrate was discarded because it might include adsorption from the dead-end cell.[47] The second hour of the filtrate was collected and analyzed with a UV−vis spectrophotometer (Thermo Scientific Genesys 10S). Dye rejection is defined by eq 5

$$\text{rejection}(\%) = \left(1 - \frac{A_p}{A_f}\right) \times 100 \quad (5)$$

where A_f is the feed absorbance, and A_p is the permeate absorbance. The absorbance of MO and MB was measured at their peak wavelengths (λ_{max}), which are 465 and 665 nm,[47] respectively. Calibration curves for both dyes were also prepared, and the linear regression between absorbance and dye concentration was confirmed. Three samples from the as-prepared, salt-annealed membranes and the control were tested.

Evaluation of Bacteria Adhesion to Membranes Using a Static Assay. Consistent with our previous reports, the Gram-negative microorganism *E. coli* containing a green fluorescent protein (GFP) plasmid was used in static bacteria fouling assays.[48,49] Overnight cultures of *E. coli* were inoculated in Luria−Bertani broth with spectinomycin (1 μL mL^{-1}) for 16 h at 37 °C, resuspended in M9 media to a concentration of 10^7 CFU/mL. Static fouling resistance tests were conducted on the as-prepared, salt-annealed, Sartorius control membranes and internal glass controls by placing them in separate wells of six-well polystyrene plates and exposing them to 5 mL of *E. coli* suspension without shaking for 24 h at 37 °C. Samples were then rinsed with M9 media three times to remove loosely attached cells. Visualization of the GFP plasmid containing *E. coli* was captured using a Zeiss Axio Imager A2M Microscope (Carl Zeiss Microscopy, White Plains, NY). Random images (n = 15) were acquired over three parallel replicates and analyzed using ImageJ software to calculate the bacteria area coverage.[45]

Statistics. All statistical significance was determined using a two-tailed, unpaired student t-test. Error bars shown throughout the results are standard deviations unless specified. Three (***), two (**), and one asterisk (*) denote that the values significantly differ at the 0.001, 0.01, and 0.05 levels, respectively. n.s. indicates that the samples are not statistically different.

RESULTS AND DISCUSSION

The NIPS process manufactures robust membranes using neutral polymers and aprotic solvents. Here, we explore using the same processing steps, i.e., immersing a cast polymer film in a nonsolvent bath but substituting a single-phase coacervate dope solution, to develop robust, high-performance membranes via APS. We first explored the concentration of salt (KBr) in the membrane-casting dope solution (i.e., coacervate) and the coagulation bath. We assess the success of changing the salt concentration by analyzing the formed membranes' pore structure and PWP. Then, we introduce salt annealing post-treatment to determine how it affects membrane filtration performance such as rejecting PEG and dye molecules. Finally, by depositing *E. coli* bacteria onto the surface of the PEC

https://doi.org/10.1021/acsami.4c18989
ACS Appl. Mater. Interfaces XXXX, XXX, XXX−XXX

membranes, we investigate the ability of the membranes' surface to repel microorganisms.

Impact of Coacervate Composition on Membrane Structure and Performance. We first studied the effect of the coacervate KBr concentration on membrane formation, and the compositions explored are provided in Table 1. We note that KBr concentrations lower than 1.4 M were too viscous to be cast, while concentrations higher than 1.6 M were too watery/runny, preventing stable casting. A thin, homogeneous coacervate layer (PSS to PDADMAC at a monomer ratio of 1 to 1) containing varied KBr concentrations (1.4, 1.5, and 1.6 M) was successfully cast into consistent films. These cast films were immersed in a 0.4 M $KBr_{(aq)}$ coagulation bath. The as-prepared membranes will be referred to as 1.4/0.4, 1.5/0.4, and 1.6/0.4, where the first value is the coacervate KBr concentration (M) and the second value is the KBr concentration (M) in the coagulation bath. Using rheology, we determined that the zero shear viscosities of the three coacervates, 1.4, 1.5, and 1.6 M, that resulted in successfully cast membranes were 34.5 ± 2.0, 4.9 ± 0.1, and 0.77 ± 0.06 P, respectively, as provided in Table S1. Our 1.5 M coacervate had a similar viscosity to a 15 wt % polysulfone in an NMP solution, which has previously been reported to have a viscosity of 3.1 P and has been cast into phase inversion membranes using the NIPS process.[50]

Top-down, cross section, and enlarged cross-sectional SEM micrographs of the membranes are shown in Figures 1 and S1. No visible pores were observed on the surface of the 1.4/0.4 and 1.5/0.4 membranes, whereas we started to see small pinholes on the 1.6/0.4 membranes. All cross-sectional micrographs revealed an asymmetric pore structure, where the sponge-like interconnected substructure and dense skin-layer morphology indicate successful membrane fabrication. Though no macrovoids were observed for these membranes, 1.5/0.4 and 1.6/0.4 showed signs of inconsistent morphology and possibly delamination near the upper part of the porous substructure, which might lead to decreased mechanical stability. The dry thickness of the dense skin layer varied between 1.29 and 1.58 μm, as measured using ImageJ from SEM micrographs, as summarized in Table S2. Overall, visually the morphologies of the three membranes did not substantially differ from each other.

The precipitation mechanism of APS is similar to NIPS:[29,30] as the solution viscosity increases, the onset of the precipitation is delayed, resulting in smaller pore sizes and denser structures. To date, only one paper has utilized the coacervate phase to fabricate membranes via the APS process.[40] Sadman et al. explored the PSS/poly(*N*-ethyl-4-vinylpyridinium) (QVP-C2)/KBr polyelectrolyte coacervate system, where the coacervate KBr concentration was varied from 15.1 to 18.3 wt %. With increasing KBr concentration, the skin layer transitioned from completely dense to having 10−100 nm pores. Moreover, the thickness of the skin layer increased significantly with a decreasing KBr concentration. The kinetics of precipitation can again explain the morphological changes. When the coacervate salt concentration increases, the polyelectrolyte concentration decreases with an increasing water content. Most importantly, coacervate viscosity increases with decreasing salt concentration.[11,51] The restricted polyelectrolyte chain mobility and higher polyelectrolyte concentration eventually lead to a thicker skin layer and a lower overall porosity. However, the dry thickness of the skin layer and the overall porosity of our as-prepared membranes seemed very similar; we note that these observations were made under vacuum using SEM, post-preparation via liquid nitrogen flash freezing, and cracking.

We found that the membranes' wet thickness, which is rarely reported, decreased with higher KBr concentration, as summarized in Figure 2a. The wet thicknesses of the as-prepared 1.4/0.4, 1.5/0.4, and 1.6/0.4 PEC membranes, including the nonwoven support (135 μm), were 227, 197, and 181 μm, respectively. As the KBr concentration decreased, the polymer concentration and viscosity of the casting dope increased (see Table S1), and the overall porosity of the membrane was expected to decrease.[52] The 1.4/0.4 membrane with a higher polymer concentration would be expected to retain their structure during precipitation better and to have the greatest overall thickness. On the other hand, during and after precipitation, the 1.6/0.4 membrane pores could undergo more compaction when they theoretically should possess higher porosity. Casting higher KBr concentrations and lower polyelectrolyte content can potentially reduce the mechanical stability of a porous substructure.

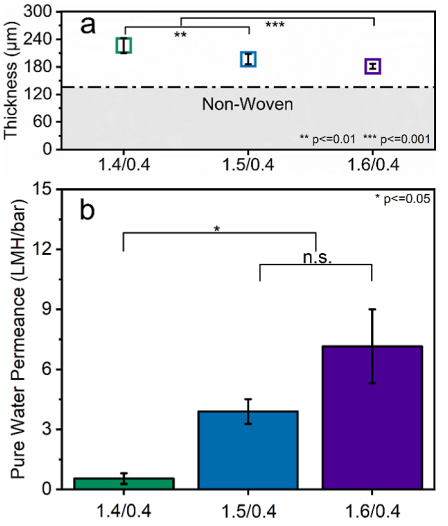

Figure 2. (a) Wet thickness and (b) PWP of the as-prepared PEC membranes prepared from varied coacervate KBr concentrations (1.4, 1.5, and 1.6 M) in a 0.4 M $KBr_{(aq)}$ coagulation bath. Wet thickness includes the 135 μm thick nonwoven substrate. Values of wet thickness and PWP are summarized in Table S3.

PWP tests were conducted at 3 bar with a dead-end filtration setup to investigate the membrane performance. The PWP of the 1.4/0.4, 1.5/0.4, and 1.6/0.4 membranes was determined to be 0.81, 3.9, and 7.2 L m^{-2} h^{-1} bar^{-1}, respectively; see Figure 2b and Table S3. The PWP increased with decreasing membrane thickness, which could result from lower water transport through the porous substructure.[52] Even though the skin layer thickness did not change significantly, the surface porosity could increase with decreased polymer concentration in the coacervate solution, the confirmation of which would require further characterization beyond this study's scope. The larger standard deviation demonstrated by the 1.6/0.4 membranes suggests that their pore structure was less mechanically stable, whereas the 1.4/0.4 membranes showed a lower but the most consistent performance, benefiting from the delamination-free structure. However, their PWP was quite low for reasonable nanofiltration applications, which likely resulted from the high viscosity and high polymer concen-

https://doi.org/10.1021/acsami.4c18989
ACS Appl. Mater. Interfaces XXXX, XXX, XXX−XXX

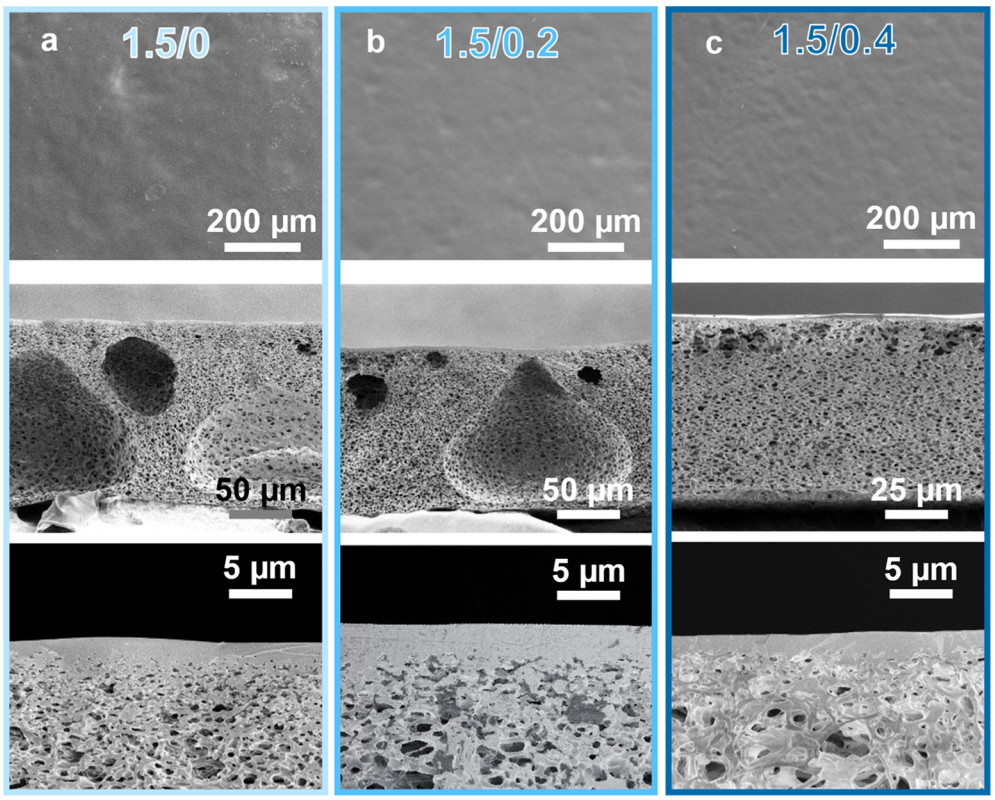

Figure 3. (top row) Top-down, (middle row) cross-sectional, and (bottom row) enlarged cross-sectional SEM images of the PSS/PDADMAC membranes prepared from 1.5 M KBr containing coacervates in varied coagulation bath KBr concentrations of (a) 0 (pure water), (b) 0.2, and (c) 0.4 $M_{(aq)}$. Dry membrane and skin layer thickness are summarized in Table S2.

tration of the 1.4 M KBr coacervate dope solution. Therefore, membranes cast from 1.5 M KBr coacervate will be used throughout the rest of the study.

Impact of Coagulation Bath Salinity on Membrane Structure and Performance. So far, we have selected the optimized coacervate KBr concentration, but we note that the coagulation bath salinity is another crucial membrane fabrication parameter. Typically, the coacervate film solidifies and turns white immediately upon immersion in the coagulation bath, and the appearance of the membrane surface remains unchanged after the first 10 min. Notably, a KBr concentration higher than 1.0 M did not create a sufficient driving force for complete salt ion removal. Macroscopic images of membranes after precipitation can be found in Figure S2, where the coacervate precipitated in 1.0 M $KBr_{(aq)}$ solution retains its transparent, viscous-like appearance. Therefore, we focused on using the membranes cast from the optimized 1.5 M KBr coacervates and immersed them in 0 (pure water), 0.2, and 0.4 M $KBr_{(aq)}$ coagulation baths, which will be referred to as 1.5/0, 1.5/0.2, and 1.5/0.4, respectively (Table 1). Notably, membranes cast from 1.4 to 1.6 M KBr coacervates were also precipitated in all three bath salinities. However, the 1.4 M KBr showed minimal PWP, and the 1.6 M KBr showed poor mechanical stability; therefore, neither was further characterized.

Figure 3 shows the SEM images of cast membranes postsubmersion in coagulation baths with different salinities. No visible pores were found on the surface of any of these membranes. We also observed that all membranes had an asymmetric structure with a dense skin layer but with different substructure morphologies. The 1.5/0 and 1.5/0.2 membranes both contained "water-drop-like" macrovoids within the substructure, indicating an instantaneous demixing mechanism with a relatively high precipitation rate.[30,36] However, for the 1.5/0.4 membranes, a sponge-like morphology with open interconnected pores was observed, indicating a slower, delayed demixing mechanism. The salt ions in the coagulation bath likely limited the release of counterions from the polyelectrolytes, whereas a higher coagulation bath salinity would create a slower precipitation rate resulting in a less porous structure. Also, the presence of salt within the bath increases the chain mobility of the polyelectrolytes, especially near the membrane's surface. Thus, the polyelectrolyte chains can better associate during precipitation, creating a denser and thicker skin layer.[29,30]

Visually, we did not observe a substantial difference in the dense layer's porosity or thickness from changing the coagulation bath salinity. Again, we report that the wet membrane thickness decreased with increasing bath salinity; the wet thickness is summarized in Figure 4a and Table S3. The wet thicknesses of the 1.5/0, 1.5/0.2, and 1.5/0.4 membranes were 243, 236, and 197 μm, respectively. The PWP of the 1.5/0, 1.5/0.2, and 1.5/0.4 membranes again increased with decreasing wet thicknesses, which were 0.33, 0.34, and 3.9 L m^{-2} h^{-1} bar^{-1}, respectively. The thinner wet thickness of the 1.5/0.4 membrane could contribute to its highest PWP value; however, membrane compaction might be the dominating factor. It is possible that the macrovoids in the 1.5/0.2 and 1.5/0.4 structures would simply collapse during filtration, which would lead to a more compact structure and result in minimal PWPs. This is supported by the additional 10% reduction in average wet thickness (excluding nonwoven)

https://doi.org/10.1021/acsami.4c18989
ACS Appl. Mater. Interfaces XXXX, XXX, XXX−XXX

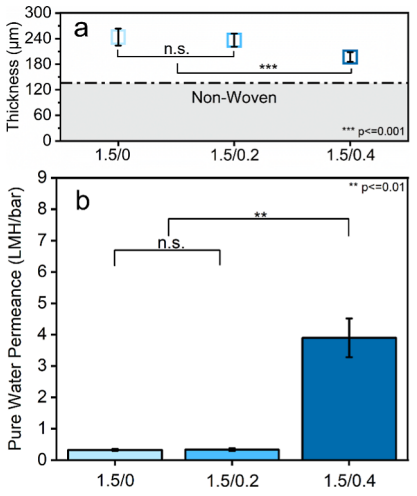

Figure 4. (a) Wet thickness and (b) PWP of the PSS/PDADMAC membranes prepared from 1.5 M KBr containing coacervate in varied coagulation bath KBr concentrations [0 (pure water), 0.2, and 0.4 $M_{(aq)}$]. Wet thickness includes the 135 μm thick nonwoven substrate. Values of wet thickness and PWP are summarized in Table S3.

for the 1.5/0.2 compared to the 1.5/0.4 membranes after PWP (as detailed in Table S3). In conclusion, the 0.4 M $KBr_{(aq)}$ coagulation bath salinity, along with the 1.5 M KBr coacervate salt concentration, yielded membranes that provided the most stable, consistent, and reasonable PWP for nanofiltration applications, which will be used in further studies.

Impact of Salt Annealing on Membrane Structure and Performance. Coacervate materials are saloplastic, and previous literature has used salt postprocessing methods to decrease the roughness and enhance the performance of other polyelectrolyte-containing materials.[41−43] Thus, we post-treated the optimized 1.5/0.4 membranes using a 1.6 M NaCl water bath. This method was selected because PSS/PDADMAC complexes are known to undergo a glass transition at NaCl concentrations higher than 1.5 M or temperatures higher than 45 °C, which allows the polyelectrolyte chains to rearrange.[53−56]

SEM images of the salt-annealed membranes are shown in Figure 5a, where the membrane morphologies did not show a significant difference from the as-prepared 1.5/0.4 membranes, shown in Figures 3c and S3. Cross-sectional images suggest that they have an asymmetric pore structure, and notably, we noticed that the skin layer thickness increased from 1.44 to 5.15 μm after annealing, possibly resulting from polyelectrolyte chain rearrangement near the membrane surface. The dry and wet thicknesses and PWP performances are summarized in Table S2 and Figure 5b,c. The average wet thickness showed an increase from 197 to 203 μm after annealing, though this was not a statistically relevant change. The average PWP did increase from 3.9 to 6.2 L m^{-2} h^{-1} bar^{-1}. Several factors from salt-annealed PEM studies explain that the swelling or hydration ratio increases after annealing. First, salt annealing of PEMs at a high ionic strength is shown to favor compensation by counterions, shifting intrinsic compensation (oppositely charged polyelectrolytes) toward extrinsic compensation (charged balanced by counterions). This transition will increase the charge density, as well as the degree of swelling that leads to a more hydrated PEM layer.[43,57] PDADMAC-terminated PSS/PDADMAC PEMs have been reported to have a higher swelling degree than PSS-terminated films, making the multilayer less dense.[43,55] Recently, Kamp et al. found that PDADMAC overcompensation occurred in APS membranes, even when preparing membranes from equimolar PSS and PDADMAC, the surface zeta potential was ∼+5 mv.[36]

The annealing of our membranes could pull the excess PDADMAC to the surface, leading to an even more net-positive membrane and, thus, a higher hydration ratio.[41,55] In our case, given the fact that the membrane morphology did not change significantly, the effect of salt annealing on PWP was expected to be minimal. A slight (but not statistically relevant) increase in the PWP suggests that a more hydrated and less

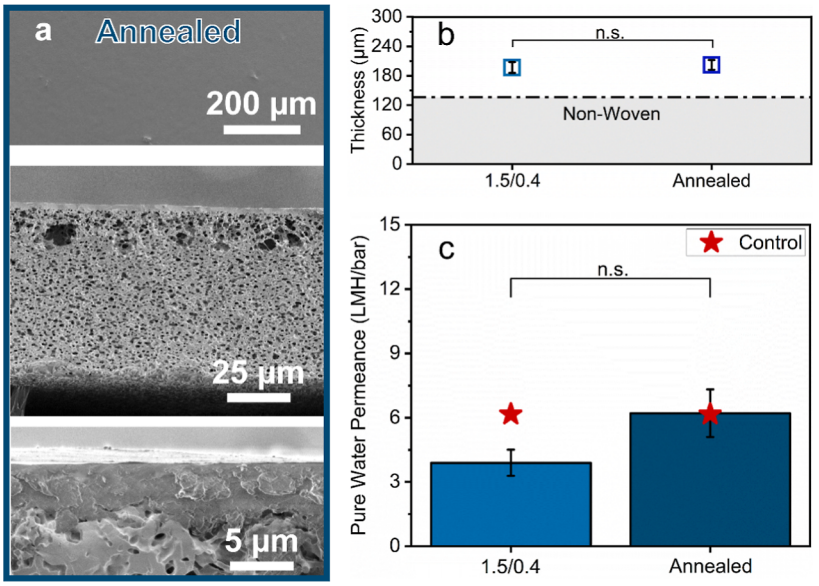

Figure 5. (a) (top row) Top-down, (middle row) cross-sectional, and (bottom row) enlarged cross-sectional SEM images of the 1.5/0.4 membrane structure annealed in 1.6 M $NaCl_{(aq)}$ solution. (b) Wet thickness and (c) PWP of the membranes before and after salt annealing. The PWP of the Sartorius control membrane is displayed using a red symbol; n.s. indicates that the samples are not statistically different. Values of dry and wet thickness and PWP are summarized in Tables S2 and S3.

https://doi.org/10.1021/acsami.4c18989
ACS Appl. Mater. Interfaces XXXX, XXX, XXX−XXX

dense membrane was obtained after annealing, even with a thicker skin layer. The PWP value after annealing was nearly identical to the commercial control membrane, shown in the red symbol in Figure 5c. Notably, an increase in the hydration ratio was not found in membranes fabricated under different conditions. For example, the average thickness of 1.5/0.2 membranes decreased by 30%, potentially because the relatively unstable macrovoids compressed or even collapsed during chain rearrangement. Further investigations into how salt annealing can affect different membrane morphologies are needed.

Effect of Using a Single-Phase Coacervate as the Dope Solution. Until now, we have not discussed how utilizing the coacervate phase (polymer-rich phase) differs from using an overcritical one-phase solution as a casting solution. Here, we will compare the results reported by Kamp et al., where they fabricated ultrafiltration and NF membranes from different PSS/PDADMAC monomer ratio solutions and used a DI water coagulation bath.[36] First, the morphologies and PWPs of 50:50 and 55:45 membranes were similar to our 1.5/0.4 membrane, where a dense skin layer formed on top of a porous interconnected substructure showing an NF PWP range. Since the coacervate phase represents a distinct point on the binodal curve, the demixing starts immediately when the cast film enters the coagulation bath, leading to rapid polymer complexation and formation of a more porous skin layer. In this work, to achieve delayed demixing within the coacervate phase, we raised the coagulation bath salinity to 0.4 M, whereas only water was needed for the overcritical casting solution. Therefore, the coacervate phase had a smaller coagulation bath salinity window and might be more sensitive to salinity changes in the bath.

In the article by Wang et al., despite starting from an equal PDADMAC to PSS molar ratio, they found that the PDADMAC content in the polymer-lean phase was higher, possibly because KBr is a better solvent for PDADMAC than PSS.[11] Here, we are using the coacervate phase as a casting solution and the PSS to PDADMAC ratio is close to 1.1 to 1. According to Wang et al., this could also explain why the 1.5/0.4 membrane properties are similar to those of the 55:45 membrane. Furthermore, Kamp et al. hypothesized that the demixing and excess of PDADMAC in the polymer-lean phase would lead to a chemical gradient potential that allows PDADMAC to diffuse to the surface, thus, resulting in overcompensation. The surface zeta potential for the 55:45 membrane was between +20 and +30 mV with varied pH values, whereas the 1.5/0.4 membrane was +63 mV at pH = 5, as presented in Figures S4 and S5 and Table S4. The excess PDADMAC on the surface leads to a positive surface charge, which is in accordance with previous studies. However, excess PDADMAC is also known to make the complex rubbery, possibly compromising the membranes' long-term stability.[43] Finally, the PWPs of the 50:50 and 55:45 membranes were significantly lower (<0.5 L m^{-2} h^{-1} bar^{-1}) than the 1.5/0.4 (3.9 L m^{-2} h^{-1} bar^{-1}) membranes, possibly resulting from delayed demixing. In conclusion, the instantaneous demixing nature of the coacervate could create a more porous structure, thus giving a higher PWP value. However, the long-term stability of the 1.5/0.4 membrane would need further investigation, given its even higher net positive surface charge.

Separation Performance of Optimized Coacervate Membranes. To characterize the separation capability of our membranes, model neutral PEG (600, 1k, and 2k Da) and two oppositely charged dye molecules with similar molecular weight, MB and MO, were selected to ascertain the roles of solute size and charge effects. Specifically, MB is cationic with a M_w = 320 g/mol, whereas MO is anionic with a M_w = 327 g/mol.[47,58]

The rejection of the neutral PEG molecules is summarized in Table 2. The control showed the highest rejection for all three PEG molecular weights, while the annealed membrane had the lowest rejection. Previous studies have shown that the commercial PES 1 kDa control membranes demonstrated widespread rejections at their molecular weight cutoff (MWCO). This indicates a large pore size distribution and a lack of precise size-based selectivity.[47] This was again observed as the rejection of 1 kDa PEG by the commercial control membranes was 57.3%, which is significantly lower than the expected 90% rejection cutoff. With all membranes having an MWCO larger than 1 kDa, the 1.5/0.4 and annealed membranes fall into the tight-ultrafiltration category.[59] The decrease in all three PEG rejections after salt annealing potentially resulted from a more hydrated, less dense skin layer with a higher PWP.

Table 2. Rejection of PEG as a Function of Molecular Weight Using 1.5/0.4, Annealed, and Control Membranes[a]

membrane	PEG rejection (%)		
	M_W = 2000 Da	M_W = 1000 Da	M_W = 600 Da
1.5/0.4	54.1 ± 8.8	37.0 ± 3.6	13.6 ± 7.8
annealed	34.5 ± 7.7	29.3 ± 6.9	6.7 ± 7.8
control	89.4 ± 2.8	57.3 ± 7.0	49.7 ± 4.8

[a]Average values and standard deviations are provided.

Ion-containing membranes are commonly used to remove charged contaminants, such as dye molecules, via adsorption, charge repulsion, and size-sieving mechanisms.[60−65] Single-component adsorption tests were conducted to investigate the adsorptive contribution to the dye rejection mechanism. Figures 6a,b and S6 show that 1.5/0.4 and annealed membranes adsorbed 31% and 36% of MO in 4 h, and up to 67% and 78% after 24 h, respectively. Interestingly, all membranes showed negligible adsorption of MB after 24 h. The membrane color change after 4 h of adsorption experiments, shown in Figure S7, was in accordance with the

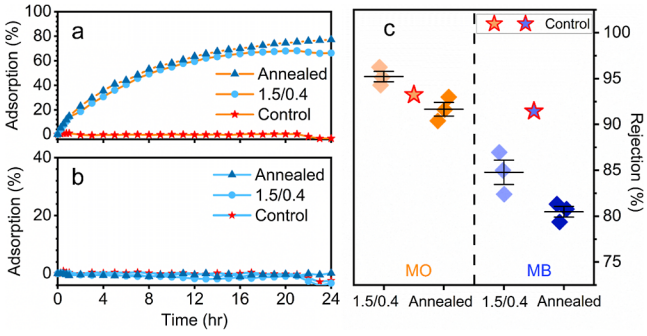

Figure 6. Single-component adsorption results show the (a) MO and (b) MB adsorption percentage as a function of time in the presence of 1.5/0.4, annealed, and control membrane. (c) Steady-state MO and MB dye rejection percentages for 1.5/0.4, annealed, and control membranes are shown in scatter plots. Values of dye rejection and standard deviations are summarized in Table S4.

https://doi.org/10.1021/acsami.4c18989
ACS Appl. Mater. Interfaces XXXX, XXX, XXX−XXX

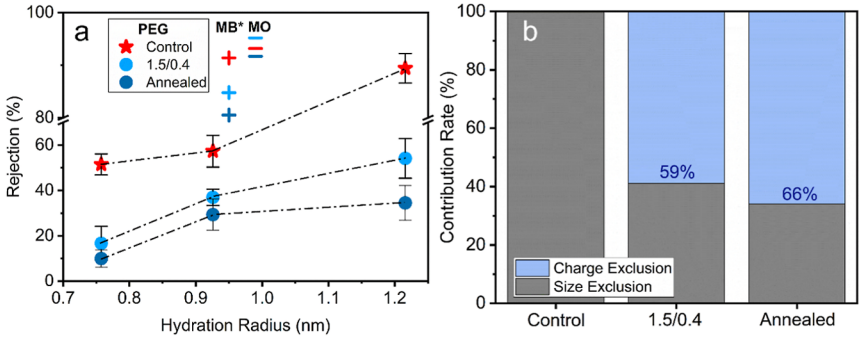

Figure 7. (a) Neutral (PEG) and charged (MO, MB) solute rejection as a function of hydration radius. MB* indicates that while MO and MB are similar in size, MB is shifted to the left for clarity. (b) Estimated contribution rate of size-based and charge-based exclusion to membrane dye rejection.

surface zeta potential and adsorption results: cationic PEC membranes stained orange in anionic MO but maintained their original white appearance after immersion in cationic MB solution. The excess PDADMAC of the 1.5/0.4 membranes and the additional charges induced by salt annealing likely created positive sites for anionic MO to adsorb.[36,41] On the other hand, the control membranes stayed light yellow and blue after the adsorption experiments, indicating that minimal adsorption by MO and MB had occurred. It is known that first, the adsorption of hydroxide ions occur, which creates available negative sites on commercial PES membranes under alkaline conditions. The acidic MO and MB would limit the creation of negative charge sites and keep PES close to its isoelectric point, minimizing both MB and MO adsorption.[66] Therefore, we expect charge-based exclusion to have a minor dominance on control membranes.

To further evaluate the performance of the PEC membranes, a solution containing 50 ppm each of MB and MO was filtered through the as-prepared 1.5/0.4, annealed, and control membranes. To eliminate the contribution of adsorption to dye rejection, membranes were immersed and saturated in the feed solution for 24 h before steady-state dye separation tests. Figure S8 shows the UV−vis spectra of each of the dyes as well as the feed and permeates of the three tested membranes. The characteristic peak of MO at 465 nm is less visible than that of MB at 665 nm, showing higher retention and separation of the anionic dye for all membranes. Figure S9 shows that the color of the PEC membranes turned from white to orange, whereas the control changed from white to green after 2 h of rejection tests, which again aligns with the observation after saturation adsorption. Figure 6c and Table S4 show a closer look at the tested samples' dye rejection percentages. The 1.5/0.4, annealed, and control membranes rejected 95.2, 91.7, and 93.2% MO, while 84.8, 80.5, and 91.4% MB were rejected, respectively. First, the MO and MB rejections decreased by 3.5% and 4.3% for membranes after annealing, respectively. This likely resulted from the more hydrated, less dense skin structure with a higher PWP, in accordance with the decreased PEG rejection after salt annealing. Furthermore, by comparing dye rejection results collected before (nonsteady state) and after 24 h of saturated adsorption, it can be observed that the MO rejection decreased by only 1.5% and 5.0% for 1.5/0.4 and annealed membranes, respectively, which is significantly lower than the single-component adsorption results, which adsorbed around 20% in just 2 h; see Figure S10 and Table S5. On the other hand, MB rejection increased by 5.1, 5.0, and 1.8% for 1.5/0.4, annealed, and control membranes, respectively. Increased size exclusion after saturation might be the main factor. Since the PEC cationic charges were expected to neutralize after saturation, the increase in the cationic MB rejections cannot be explained by charge repulsion. Even though MO and MB rejection results showed that charge-based exclusion might have played a minor role, especially after saturation,[60] rejections based on hydration radius might suggest otherwise.

Figure 7a shows the neutral and charged solute rejections as a function of the hydration radius. Molecular dynamics simulation estimated MO to be 0.99 nm.[62] While studies have shown that the molecular sizes of MO and MB are very similar,[67] for clarity, in Figure 7, MB was offset from MO. Even after accounting for the bulky dye molecules' steric hindrance, both 1.5/0.4 and annealed membranes showed a significantly higher rejection over the similar-size 1k Da PEG molecules, suggesting that charge-based exclusion still plays a significant role even after saturated adsorption. The probable reason is that dye adsorption can be surface-based and can be limited by diffusion. At the same time, during filtration, convective mass transport allows more charge sites to be available for MO and MB on the membranes' surface and pores.[66] Therefore, the membranes did not reach their maximum adsorption capacity after saturation, and the positive charge on the PEC membranes was not completely neutralized. Donnan exclusion and adsorption can still contribute to the removal of MB and MO, respectively. However, MO showed a 10% higher rejection over MB for both 1.5/0.4 and annealed membranes. It is possible that the protonated N double bond presence in MO at an acidic pH could form a strong chemical interaction in the form of hydrogen bonding with the sulfonic acid group on PSS, which can further improve the rejection of MO in addition to electrostatic attraction.[61]

The estimated contribution rate of size-based and charge-based exclusion mechanisms of charged solutes is presented in Figure 7b. The size-based contribution was obtained from rejecting 1 kDa PEG molecules, given their similar hydration ratio to both charged dye molecules. On the other hand, the charge-based contribution was obtained from the average of MO and MB rejection after subtracting the 1 kDa PEG rejection rate. Since the control membranes showed a 90% cutoff for solutes around 1 nm, regardless of charge, and minimal preferential electrostatic interaction to charged dyes, size exclusion is the dominating mechanism. However, after 24 h of dye adsorption, PEC membranes still demonstrated up to 59 and 66% charge-based exclusion. The increase in charge-based exclusion or decrease in size-based exclusion after

https://doi.org/10.1021/acsami.4c18989
ACS Appl. Mater. Interfaces XXXX, XXX, XXX−XXX

annealing was primarily due to the more hydrated, less dense skin layer that resulted in potentially larger pore sizes. In conclusion, size- and charge-based exclusion mechanisms contributed to the separation performance of PEC membranes.

Static Resistance to Bacteria Deposition by Coacervate Membranes. The resistance to bacterial fouling on the surface of the 1.5/0.4, annealed, and control membranes was evaluated using *E. coli* using a well-established static assay.[49] The results are shown in Figure 8. Compared to glass slides (internal control), the 1.5/0.4, annealed, and control membranes all showed reduced *E. coli* adhesion, with values of 1.45% to 0.48%, 0.30%, and 0.12%, respectively. Evaluation using these static tests showed that all three membranes tested, the commercial controls, 1.5/0.4, and annealed membranes, had statistically equivalent area coverage by *E. coli*. While the hydrophilicity and proximity of positive and negative charges within the PEC likely prevent bacteria from adhering to the as-prepared membranes,[68] poly(ether sulfone) control membranes have been reported by the manufacturer to "exhibit no hydrophobic or hydrophilic interactions and are usually preferred for their low fouling characteristics".[69] We note that these experiments were surface-based evaluations, and thus, they do not provide performance comparisons before and after PWP experiments, such as flux recovery ratio, which was beyond the scope of this work but should be conducted in the future.

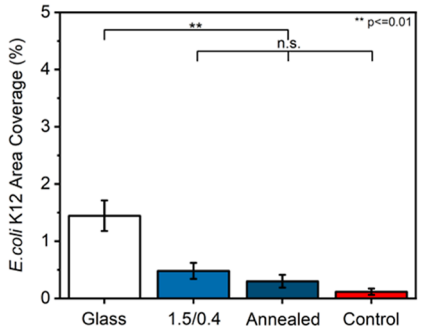

Figure 8. *E. coli* area coverage of glass, 1.5/0.4, annealed, and control membranes after 24 h of incubation at 37 °C. Error bars denote standard errors. Two asterisks (**) denote that the values significantly differ at the 0.01 level, whereas n.s. indicates that the samples are not statistically different. Values of *E. coli* area coverage are summarized in Table S4.

In addition to their difference in chemistry, the membranes' surface roughness could also influence their propensity to foul. Table S6 and Figure 9 summarize the AFM roughness data and representative height profile images of the 1.5/0.4, annealed, and control membranes. The control commercial membranes offer the lowest average surface roughness (Ra = 8.9 ± 8.3 nm) and a negatively charged surface amenable to repelling the negatively charged *E. coli* cells.[70] The average surface roughness (Ra) of the 1.5/0.4 membrane was 42.4 ± 14.8 nm and did not change significantly after annealing, which was determined to be 40.4 ± 13.0 nm. Therefore, further optimization of surface roughness and charge could produce smoother membranes with an even greater resistance to adhesion by molecules and foulants.

CONCLUSIONS

In this study, we successfully utilized the sustainable APS method to fabricate a mechanically stable PSS/PDADMAC complex membrane from a polymer-rich coacervate dope solution for the first time. The effect of salt annealing, coagulation bath salinity, and KBr concentration in the dope casting solution on membrane thickness, structure, and performance was systematically investigated. The annealed membranes' PWP and rejection of MO and MB were comparable to commercial poly(ether sulfone) nanofiltration membranes with a molecular weight cut off at 1000 Da. Interestingly, we found that charge-based exclusion mechanisms likely contribute up to 66% of the dye rejection, even after saturated adsorption for the cationic PEC membrane, making size and charge exclusion both dominating factors. Furthermore, the static resistance to *E. coli* attachment was also demonstrated for the first time, and coacervate membranes repelled bacteria at the same level as the commercial control membranes. In future work, long-term dynamic fouling and flux recovery performance need to be investigated. However, these experiments are beyond the scope of this work, which establishes an optimized method of preparing APS membranes from a single-phase coacervate solution. In conclusion, this work paves the way for future exploration of using polyelectrolyte coacervates as the dope solution to fabricate biofouling-resistant and mechanically stable water filtration membranes without the use of any solvents.

ASSOCIATED CONTENT

Supporting Information

The Supporting Information is available free of charge at https://pubs.acs.org/doi/10.1021/acsami.4c18989.

Rheology method and viscosity data; membrane dry and wet thickness; digital images of cast membranes; cross-sectional SEM images; summary of membrane performance properties; surface zeta potential measurements;

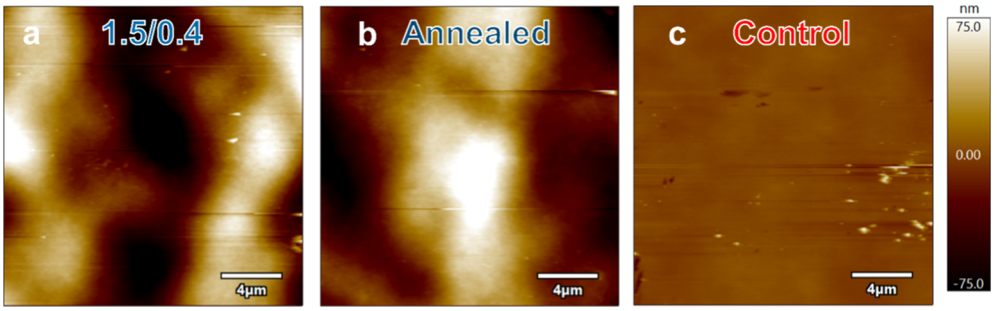

Figure 9. Representative AFM height profile images of (a) 1.5/0.4, (b) annealed, and (c) control membranes. Table S6 provides a comprehensive summary of the surface roughness measurements that were determined from AFM measurements.

https://doi.org/10.1021/acsami.4c18989
ACS Appl. Mater. Interfaces XXXX, XXX, XXX−XXX

dye adsorption and rejection images and data; and AFM surface roughness data (PDF)

AUTHOR INFORMATION

Corresponding Author

Jessica D. Schiffman − *Department of Chemical Engineering, University of Massachusetts Amherst, Amherst, Massachusetts 01003-9303, United States;* orcid.org/0000-0002-1265-5392; Email: schiffman@umass.edu

Authors

Shao-Hsiang Joe Hung − *Department of Chemical Engineering, University of Massachusetts Amherst, Amherst, Massachusetts 01003-9303, United States;* orcid.org/0000-0001-8160-2668

Meng-Chen Chiang − *Department of Chemical Engineering, University of Massachusetts Amherst, Amherst, Massachusetts 01003-9303, United States;* orcid.org/0009-0003-3620-1533

Complete contact information is available at: https://pubs.acs.org/10.1021/acsami.4c18989

Notes

The authors declare no competing financial interest.

ACKNOWLEDGMENTS

The authors acknowledge the support of the National Science Foundation (award number 2227307). We acknowledge the use of the UMass Amherst Biophysical Characterization Core Facility, RRID:SCR_022357, and the W.M. Keck Center for Electron Microscopy. We thank Prof. Stephen S. Nonnenmann for use of their AFM, Dr. Stephen Call and Prof. Lauren Andrews for green fluorescent protein-labeled *E. coli*, and Grace Leone and Prof. Todd Emrick for use of the SEC/GPC.

ABBREVIATIONS

AC, alternating current; AFM, atomic force microscope; APS, aqueous phase separation; DI, deionized; DMF, dimethylformamide; *E. coli*, *Escherichia coli*; GFP, green fluorescent protein; KBr, potassium bromide; LB, Luria−Bertani; MB, methylene blue; M_w, molecular weight; MO, methyl orange; NaCl, sodium chloride; NF, nanofiltration; NIPS, nonsolvent-induced phase separation; NMP, *N*-methyl-pyrrolidine; PDADMAC, poly(diallyldimethylammonium chloride); PEC, polyelectrolyte complex; PEG, poly(ethylene glycol); PEMs, polyelectrolyte multilayers; PSS, poly(sodium 4-styrenesulfonate); PWP, pure water permeance; QVP-C2, poly(*N*-ethyl-4-vinylpyridinium); RO, reverse osmosis; SEM, scanning electron microscopy; TMP, transmembrane pressure

REFERENCES

(1) *Summary Progress Update 2021 − SDG 6 − Water and Sanitation for All*, 2021. https://www.unwater.org/sites/default/files/app/uploads/2021/12/SDG-6-Summary-Progress-Update-2021_Version-July-2021a.pdf (accessed 2023−11−09).

(2) Qasim, M.; Badrelzaman, M.; Darwish, N. N.; Darwish, N. A.; Hilal, N. Reverse Osmosis Desalination: A State-of-the-Art Review. *Desalination* **2019**, *459*, 59−104.

(3) Hayama, M.; Yamamoto, K.; Kohori, F.; Sakai, K. How Polysulfone Dialysis Membranes Containing Polyvinylpyrrolidone Achieve Excellent Biocompatibility? *J. Membr. Sci.* **2004**, *234* (1), 41−49.

(4) Yang, Z.; Zhou, Y.; Feng, Z.; Rui, X.; Zhang, T.; Zhang, Z. A Review on Reverse Osmosis and Nanofiltration Membranes for Water Purification. *Polymers* **2019**, *11* (8), 1252.

(5) Aroon, M. A.; Ismail, A. F.; Montazer-Rahmati, M. M.; Matsuura, T. Morphology and Permeation Properties of Polysulfone Membranes for Gas Separation: Effects of Non-Solvent Additives and Co-Solvent. *Sep. Purif. Technol.* **2010**, *72* (2), 194−202.

(6) Guillen, G. R.; Pan, Y.; Li, M.; Hoek, E. M. V. Preparation and Characterization of Membranes Formed by Nonsolvent Induced Phase Separation: A Review. *Ind. Eng. Chem. Res.* **2011**, *50* (7), 3798−3817.

(7) Wang, H. H.; Jung, J. T.; Kim, J. F.; Kim, S.; Drioli, E.; Lee, Y. M. A Novel Green Solvent Alternative for Polymeric Membrane Preparation via Nonsolvent-Induced Phase Separation (NIPS). *J. Membr. Sci.* **2019**, *574*, 44−54.

(8) Razali, M.; Kim, J. F.; Attfield, M.; Budd, P. M.; Drioli, E.; Lee, Y. M.; Szekely, G. Sustainable Wastewater Treatment and Recycling in Membrane Manufacturing. *Green Chem.* **2015**, *17* (12), 5196−5205.

(9) Substance Information—European Chemicals Agency. *ECHA Chemicals Database*. https://echa.europa.eu/substance-information/-/substanceinfo/100.011.662 (accessed 12 10, 2024).

(10) *Final Revised Unreasonable Risk Determination for N-Methylpyrrolidone (NMP)*; United States Environmental Protection Agency, 2022. https://www.epa.gov/system/files/documents/2022-12/NMP_Final%20Revised%20RD_12-12-22.pdf (accessed 11 09, 2023).

(11) Wang, Q.; Schlenoff, J. B. The Polyelectrolyte Complex/Coacervate Continuum. *Macromolecules* **2014**, *47* (9), 3108−3116.

(12) Fu, J.; Fares, H. M.; Schlenoff, J. B. Ion-Pairing Strength in Polyelectrolyte Complexes. *Macromolecules* **2017**, *50* (3), 1066−1074.

(13) Fares, H. M.; Wang, Q.; Yang, M.; Schlenoff, J. B. Swelling and Inflation in Polyelectrolyte Complexes. *Macromolecules* **2019**, *52* (2), 610−619.

(14) Sing, C. E.; Perry, S. L. Recent Progress in the Science of Complex Coacervation. *Soft Matter* **2020**, *16* (12), 2885−2914.

(15) Schaaf, P.; Schlenoff, J. B. Saloplastics: Processing Compact Polyelectrolyte Complexes. *Adv. Mater.* **2015**, *27* (15), 2420−2432.

(16) Bediako, J. K.; Mouele, E. S. M.; El Ouardi, Y.; Repo, E. Saloplastics and the Polyelectrolyte Complex Continuum: Advances, Challenges and Prospects. *Chem. Eng. J.* **2023**, *462*, 142322.

(17) Lyu, X.; Peterson, A. M. Humidity Tempering of Polyelectrolyte Complexes. *Macromolecules* **2018**, *51* (23), 10003−10010.

(18) Jurago, A. A.; Viers, R. A.; Nguyen, A. T.; Ribeiro, E. L.; Espera, A. H.; Caldona, E. B.; Advincula, R. C. On the 3D Printing of Polyelectrolyte Complexes: A Novel Approach to Overcome Rheology Constraints. *MRS Commun.* **2023**, *13* (5), 862−870.

(19) Durmaz, E. N.; Sahin, S.; Virga, E.; De Beer, S.; De Smet, L. C. P. M.; De Vos, W. M. Polyelectrolytes as Building Blocks for Next-Generation Membranes with Advanced Functionalities. *ACS Appl. Polym. Mater.* **2021**, *3* (9), 4347−4374.

(20) Glinel, K.; Déjugnat, C.; Prevot, M.; Schöler, B.; Schönhoff, M.; Klitzing, R. v. Responsive Polyelectrolyte Multilayers. *Colloids Surf., A* **2007**, *303* (1), 3−13.

(21) Li, X.; Goyens, W.; Ahmadiannamini, P.; Vanderlinden, W.; De Feyter, S.; Vankelecom, I. Morphology and Performance of Solvent-Resistant Nanofiltration Membranes Based on Multilayered Polyelectrolytes: Study of Preparation Conditions. *J. Membr. Sci.* **2010**, *358* (1), 150−157.

(22) Meng, X.; Schiffman, J. D.; Perry, S. L. Electrospinning Cargo-Containing Polyelectrolyte Complex Fibers: Correlating Molecular Interactions to Complex Coacervate Phase Behavior and Fiber Formation. *Macromolecules* **2018**, *51* (21), 8821−8832.

(23) Krishna B, A.; De Vos, W. M.; Lindhoud, S. Control over Charge Density by Tuning the Polyelectrolyte Type and Monomer Ratio in Saloplastic-Based Ion-Exchange Membranes. *Langmuir* **2023**, *39* (19), 6874−6884.

(24) Arif, M. B.; Kheawhom, S.; Dubas, S. T. Polyelectrolyte Complex Membranes as a Selective Zincate Separator for Secondary Zinc-Air Battery. *J. Energy Storage* **2023**, *74*, 109425.
(25) Ivanov, A. S.; Pershina, L. V.; Nikolaev, K. G.; Skorb, E. V. Recent Progress of Layer-by-layer Assembly, Free-Standing Film and Hydrogel Based on Polyelectrolytes. *Macromol. Biosci.* **2021**, *21* (10), 2100117.
(26) Iverson, E. T.; Legendre, H.; Schmieg, K.; Palen, B.; Kolibaba, T. J.; Chiang, H.-C.; Grunlan, J. C. Polyelectrolyte Coacervate Coatings That Dramatically Improve Oxygen Barrier of Paper. *Ind. Eng. Chem. Res.* **2022**, *61* (51), 18936−18942.
(27) Vos, W. M. d. Aqueous Phase Separation Method. U.S. Patent 11,465,103 B2, October 11, 2022. https://patents.google.com/patent/US11465103B2/en (accessed 2023−11−10).
(28) Vos, W. M. d., Willot, J. D., Nielen, W. M. Method for Creating a Porous Film through Aqueous Phase Separation. U.S. Patent 20,220,002,508 A1 January 6, 2022. https://patents.google.com/patent/US20220002508A1/en#patentCitations accessed 2023 11 10
(29) Durmaz, E. N.; Baig, M. I.; Willott, J. D.; De Vos, W. M. Polyelectrolyte Complex Membranes via Salinity Change Induced Aqueous Phase Separation. *ACS Appl. Polym. Mater.* **2020**, *2* (7), 2612−2621.
(30) Baig, M. I.; Durmaz, E. N.; Willott, J. D.; De Vos, W. M. Sustainable Membrane Production through Polyelectrolyte Complexation Induced Aqueous Phase Separation. *Adv. Funct. Mater.* **2020**, *30* (5), 1907344.
(31) Van Lente, J. J.; Baig, M. I.; De Vos, W. M.; Lindhoud, S. Biocatalytic Membranes through Aqueous Phase Separation. *J. Colloid Interface Sci.* **2022**, *616*, 903−910.
(32) Baig, M. I.; Sari, P. P. I.; Li, J.; Willott, J. D.; De Vos, W. M. Sustainable Aqueous Phase Separation Membranes Prepared through Mild pH Shift Induced Polyelectrolyte Complexation of PSS and PEI. *J. Membr. Sci.* **2021**, *625*, 119114.
(33) Baig, M. I.; Pejman, M.; Willott, J. D.; Tiraferri, A.; De Vos, W. M. Polyelectrolyte Complex Hollow Fiber Membranes Prepared via Aqueous Phase Separation. *ACS Appl. Polym. Mater.* **2022**, *4* (2), 1010−1020.
(34) Li, L.; Baig, M. I.; De Vos, W. M.; Lindhoud, S. Preparation of Sodium Carboxymethyl Cellulose−Chitosan Complex Membranes through Sustainable Aqueous Phase Separation. *ACS Appl. Polym. Mater.* **2023**, *5* (3), 1810−1818.
(35) Nielen, W. M.; Willott, J. D.; De Vos, W. M. Aqueous Phase Separation of Responsive Copolymers for Sustainable and Mechanically Stable Membranes. *ACS Appl. Polym. Mater.* **2020**, *2* (4), 1702−1710.
(36) Kamp, J.; Emonds, S.; Borowec, J.; Restrepo Toro, M. A.; Wessling, M. On the Organic Solvent Free Preparation of Ultrafiltration and Nanofiltration Membranes Using Polyelectrolyte Complexation in an All Aqueous Phase Inversion Process. *J. Membr. Sci.* **2021**, *618*, 118632.
(37) Mizan, M. M. H.; Rastgar, M.; Aktij, S. A.; Asad, A.; Karami, P.; Rahimpour, A.; Sadrzadeh, M. Organic Solvent-Free Polyelectrolyte Complex Membrane Preparation: Effect of Monomer Mixing Ratio and Casting Solution Temperature. *J. Membr. Sci.* **2023**, *668*, 121197.
(38) Durmaz, E. N.; Willott, J. D.; Mizan, M. M. H.; De Vos, W. M. Tuning the Charge of Polyelectrolyte Complex Membranes Prepared *via* Aqueous Phase Separation. *Soft Matter* **2021**, *17* (41), 9420−9427.
(39) Emonds, S.; Kamp, J.; Borowec, J.; Roth, H.; Wessling, M. Polyelectrolyte Complex Tubular Membranes via a Salt Dilution Induced Phase Inversion Process. *Adv. Eng. Mater.* **2021**, *23* (5), 2001401.
(40) Sadman, K.; Delgado, D. E.; Won, Y.; Wang, Q.; Gray, K. A.; Shull, K. R. Versatile and High-Throughput Polyelectrolyte Complex Membranes via Phase Inversion. *ACS Appl. Mater. Interfaces* **2019**, *11* (17), 16018−16026.
(41) Abtahi, S. M.; Marbelia, L.; Gebreyohannes, A. Y.; Ahmadiannamini, P.; Joannis-Cassan, C.; Albasi, C.; De Vos, W. M.; Vankelecom, I. F. J. Micropollutant Rejection of Annealed Polyelectrolyte Multilayer Based Nanofiltration Membranes for Treatment of Conventionally-Treated Municipal Wastewater. *Sep. Purif. Technol.* **2019**, *209*, 470−481.
(42) Ghostine, R. A.; Jisr, R. M.; Lehaf, A.; Schlenoff, J. B. Roughness and Salt Annealing in a Polyelectrolyte Multilayer. *Langmuir* **2013**, *29* (37), 11742−11750.
(43) Ghostine, R. A.; Markarian, M. Z.; Schlenoff, J. B. Asymmetric Growth in Polyelectrolyte Multilayers. *J. Am. Chem. Soc.* **2013**, *135* (20), 7636−7646.
(44) Yip, N. Y.; Tiraferri, A.; Phillip, W. A.; Schiffman, J. D.; Elimelech, M. High Performance Thin-Film Composite Forward Osmosis Membrane. *Environ. Sci. Technol.* **2010**, *44* (10), 3812−3818.
(45) Schneider, C. A.; Rasband, W. S.; Eliceiri, K. W. NIH Image to ImageJ: 25 Years of Image Analysis. *Nat. Methods* **2012**, *9* (7), 671−675.
(46) Kolewe, K. W.; Zhu, J.; Mako, N. R.; Nonnenmann, S. S.; Schiffman, J. D. Bacterial Adhesion Is Affected by the Thickness and Stiffness of Poly(Ethylene Glycol) Hydrogels. *ACS Appl. Mater. Interfaces* **2018**, *10* (3), 2275−2281.
(47) Bengani, P.; Kou, Y.; Asatekin, A. Zwitterionic Copolymer Self-Assembly for Fouling Resistant, High Flux Membranes with Size-Based Small Molecule Selectivity. *J. Membr. Sci.* **2015**, *493*, 755−765.
(48) Kurtz, I. S.; Sui, S.; Hao, X.; Huang, M.; Perry, S. L.; Schiffman, J. D. Bacteria-Resistant, Transparent, Free-Standing Films Prepared from Complex Coacervates. *ACS Appl. Bio Mater.* **2019**, *2* (9), 3926−3933.
(49) Ward, L. M.; Shah, R. M.; Schiffman, J. D.; Weinman, S. T. Nanopatterning Reduces Bacteria Fouling in Ultrafiltration. *ACS ES T Water* **2022**, *2* (9), 1593−1601.
(50) Han, M.-J.; Nam, S.-T. Thermodynamic and Rheological Variation in Polysulfone Solution by PVP and Its Effect in the Preparation of Phase Inversion Membrane. *J. Membr. Sci.* **2002**, *202* (1), 55−61.
(51) Sun, J.; Schiffman, J. D.; Perry, S. L. Linear Viscoelasticity and Time−Alcohol Superposition of Chitosan/Hyaluronic Acid Complex Coacervates. *ACS Appl. Polym. Mater.* **2022**, *4* (3), 1617−1625.
(52) Tiraferri, A.; Yip, N. Y.; Phillip, W. A.; Schiffman, J. D.; Elimelech, M. Relating Performance of Thin-Film Composite Forward Osmosis Membranes to Support Layer Formation and Structure. *J. Membr. Sci.* **2011**, *367* (1), 340−352.
(53) Shamoun, R. F.; Hariri, H. H.; Ghostine, R. A.; Schlenoff, J. B. Thermal Transformations in Extruded Saloplastic Polyelectrolyte Complexes. *Macromolecules* **2012**, *45* (24), 9759−9767.
(54) Saikaew, R.; Meesorn, W.; Zoppe, J. O.; Weder, C.; Dubas, S. T. Influence of the Salt Concentration on the Properties of Salt-Free Polyelectrolyte Complex Membranes. *Macromol. Mater. Eng.* **2019**, *304* (9), 1900245.
(55) Reurink, D. M.; Haven, J. P.; Achterhuis, I.; Lindhoud, S.; Roesink, E. H. D. W.; De Vos, W. M. Annealing of Polyelectrolyte Multilayers for Control over Ion Permeation. *Adv. Mater. Interfaces* **2018**, *5* (20), 1800651.
(56) Chen, Y.; Yang, M.; Shaheen, S. A.; Schlenoff, J. B. Influence of Nonstoichiometry on the Viscoelastic Properties of a Polyelectrolyte Complex. *Macromolecules* **2021**, *54* (17), 7890−7899.
(57) De Grooth, J.; Oborný, R.; Potreck, J.; Nijmeijer, K.; De Vos, W. M. The Role of Ionic Strength and Odd−Even Effects on the Properties of Polyelectrolyte Multilayer Nanofiltration Membranes. *J. Membr. Sci.* **2015**, *475*, 311−319.
(58) Oladoye, P. O.; Ajiboye, T. O.; Omotola, E. O.; Oyewola, O. J. Methylene Blue Dye: Toxicity and Potential Elimination Technology from Wastewater. *Results Eng.* **2022**, *16*, 100678.
(59) Baker, R. W.. *Membrane Technology and Applications*; 3rd ed.; John Wiley & Sons, 2004.
(60) Guo, J.; Zhang, Q.; Cai, Z.; Zhao, K. Preparation and Dye Filtration Property of Electrospun Polyhydroxybutyrate−Calcium Alginate/Carbon Nanotubes Composite Nanofibrous Filtration Membrane. *Sep. Purif. Technol.* **2016**, *161*, 69−79.
(61) Mansor, E. S.; Ali, H.; Abdel-Karim, A. Efficient and Reusable Polyethylene Oxide/Polyaniline Composite Membrane for Dye

https://doi.org/10.1021/acsami.4c18989
ACS Appl. Mater. Interfaces XXXX, XXX, XXX−XXX

Adsorption and Filtration. *Colloid Interface Sci. Commun.* **2020**, *39*, 100314.
(62) Hu, M.; Yang, S.; Liu, X.; Tao, R.; Cui, Z.; Matindi, C.; Shi, W.; Chu, R.; Ma, X.; Fang, K.; Titus, M.; Mamba, B. B.; Li, J. Selective Separation of Dye and Salt by PES/SPSf Tight Ultrafiltration Membrane: Roles of Size Sieving and Charge Effect. *Sep. Purif. Technol.* **2021**, *266*, 118587.
(63) Loh, C. Y.; Burrows, A. D.; Zhang, X.; Xie, M. Polymer of Intrinsic Microporosity Enabled pH-Responsive Adsorptive Membrane: Selectivity and Mechanism. *ACS Appl. Eng. Mater.* **2024**, *2* (2), 404−414.
(64) Sadeghi, I.; Kronenberg, J.; Asatekin, A. Selective Transport through Membranes with Charged Nanochannels Formed by Scalable Self-Assembly of Random Copolymer Micelles. *ACS Nano* **2018**, *12* (1), 95−108.
(65) Suhalim, N. S.; Kasim, N.; Mahmoudi, E.; Shamsudin, I. J.; Mohammad, A. W.; Mohamed Zuki, F.; Jamari, N. L.-A. Rejection Mechanism of Ionic Solute Removal by Nanofiltration Membranes: An Overview. *Nanomaterials* **2022**, *12* (3), 437.
(66) Zheng, L.; Su, Y.; Wang, L.; Jiang, Z. Adsorption and Recovery of Methylene Blue from Aqueous Solution through Ultrafiltration Technique. *Sep. Purif. Technol.* **2009**, *68* (2), 244−249.
(67) Liu, P.; Milletto, C.; Monti, S.; Zhu, C.; Mathew, A. P. Design of Ultrathin Hybrid Membranes with Improved Retention Efficiency of Molecular Dyes. *RSC Adv.* **2019**, *9* (49), 28657−28669.
(68) Akintola, J.; Chen, Y.; Digby, Z. A.; Schlenoff, J. B. Antifouling Coatings from Glassy Polyelectrolyte Complex Films. *ACS Appl. Mater. Interfaces* **2023**, *15* (43), 50058−50068.
(69) Ultrafiltration Membrane Discs for Sample Concentration. Lab Filtration (LF); Sartorius. https://shop.sartorius.com/us/p/polyethersulfone-ultrafiltration-membrane-discs-1-kda-mwco-10-pc/Ultrafiltration-Membrane-Discs-PES-1kDa (accessed 04 16, 2024).
(70) Li, X.; Xue, X.; Pashley, R. M. A Study of the Surface Charging Properties of a Standard Strain of *Escherichia Coli* (ATCC 11775) in Aqueous Solutions. *Colloids Surf., B* **2015**, *135*, 811−816.

https://doi.org/10.1021/acsami.4c18989
ACS Appl. Mater. Interfaces XXXX, XXX, XXX−XXX